

Article

Cost-Efficient EM-Driven Size Reduction of Antenna Structures by Multi-Fidelity Simulation Models

Anna Pietrenko-Dabrowska ^{1,*}  and Slawomir Koziel ^{1,2} 

¹ Faculty of Electronics, Telecommunications and Informatics, Gdansk University of Technology, 80-233 Gdansk, Poland; koziel@ru.is

² Engineering Optimization & Modeling Center, Reykjavik University, 102 Reykjavik, Iceland

* Correspondence: anna.dabrowska@pg.edu.pl

Abstract: Design of antenna systems for emerging application areas such as the Internet of Things (IoT), fifth generation wireless communications (5G), or remote sensing, is a challenging endeavor. In addition to meeting stringent performance specifications concerning electrical and field properties, the structure has to maintain small physical dimensions. The latter normally requires searching for trade-off solutions because miniaturization has detrimental effects on antenna characteristics, including the impedance matching, gain, efficiency, or axial ratio bandwidth. Furthermore, explicit size reduction is more demanding than optimization with respect to other figures of merit. On the one hand, it is a constrained task with acceptance thresholds set on the bandwidth, gain, etc. On the other hand, optimum solutions are normally located at the boundary of the feasible region, traversing of which is a difficult problem by itself. The necessity of using full-wave electromagnetic (EM) analysis for antenna evaluation only aggravates the problem due to high computational costs associated with numerical optimization algorithms. This paper proposes a procedure for expedited optimization-based miniaturization of antenna structures involving trust-region gradient search and multi-fidelity EM simulations, as well as implicit handling of design constraints using a penalty function approach. The assumed model management scheme is associated with the convergence status of the optimization process with the lowest fidelity model employed at the early stages of the algorithm run and the discretization density of the structure gradually increased to reach the high-fidelity level towards the end of the run. This allows us to achieve a considerable computational speedup without compromising the reliability. Our methodology is demonstrated using two broadband microstrip antennas. The obtained CPU savings exceed seventy percent as compared to the reference procedure involving high-fidelity model only.

Keywords: antenna design; compact antennas; internet of things; 5G communications; simulation-driven design; EM-based optimization; multi-fidelity simulations



Citation: Pietrenko-Dabrowska, A.; Koziel, S. Cost-Efficient EM-Driven Size Reduction of Antenna Structures by Multi-Fidelity Simulation Models. *Electronics* **2021**, *10*, 1536. <https://doi.org/10.3390/electronics10131536>

Academic Editor: Cheng Siong Chin

Received: 8 June 2021

Accepted: 23 June 2021

Published: 24 June 2021

Publisher's Note: MDPI stays neutral with regard to jurisdictional claims in published maps and institutional affiliations.



Copyright: © 2021 by the authors. Licensee MDPI, Basel, Switzerland. This article is an open access article distributed under the terms and conditions of the Creative Commons Attribution (CC BY) license (<https://creativecommons.org/licenses/by/4.0/>).

1. Introduction

Contemporary antenna systems are designed to work in demanding environments, and to meet rigorous performance criteria dictated by the needs of specific applications [1–3]. The requirements are normally concerned with both electrical and field antenna characteristics (reflection response [4], gain [5], radiation pattern [6]) and may call for the implementation of additional functionalities, e.g., multi-band operation [7], or circular polarization (CP) [8]. In the case of many emerging areas such as the Internet of Things (IoT) [9], fifth generation wireless communications (5G) [10], wearable or implantable devices [11], medical imaging [12], or wireless sensing [13,14], an additional prerequisite is a compact size. This complicates the design process because reducing physical dimensions has a detrimental effect on antenna characteristics, especially the impedance bandwidth [15], efficiency [16], pattern stability [17], or axial ratio bandwidth in the case of CP structures. Consequently, any practical design has to be a meticulously worked out compromise between the design objectives, including the miniaturization requirements.

Typically, a reduction of the antenna size is attempted at the stage of topology development, i.e., through the introduction of various geometrical alterations applied to the feeding structure [18], radiator [19], or the ground plane [20]. For example, in the case of broadband microstrip antennas, frequently implemented techniques include ground-plane slits [21], L-shape stubs [22], embedded cross slots [23], stepped-impedance feeding lines [24], or radiator slots [25]. Other methods are based on defected ground structures (DSG) [26,27], utilization of dedicated shapes of the radiating elements [28], incorporation of shorting pins between the radiator and the ground plane [29], as well as using dielectric resonators [30]. Regardless of the particular technique employed to achieve a compact structure, the antenna geometry parameters have to be carefully tuned to ensure satisfactory levels of all relevant performance figures. Given the topological complexity of miniaturized antennas, traditional tuning methods, largely based on parametric studies, are of questionable efficacy. As a matter of fact, the only adequate approach is rigorous numerical optimization [31,32]. Notwithstanding, optimization of compact structures is a challenging task. On the one hand, reliable evaluation of antenna characteristics requires full-wave electromagnetic (EM) analysis, which is computationally expensive. On the other hand, miniaturized devices are often described by a large number of parameters being a consequence of the aforementioned topological alterations [18–30]. Furthermore, reduction of the antenna size is a constrained problem. As the constraints (e.g., ensuring at least -10 dB reflection level over the assumed operating bandwidth) are costly to evaluate, and the minimum-size designs are allocated at the boundary of the feasible region, the optimization problem becomes numerically demanding. These difficulties are further aggravated by the numerical noise inherent to EM simulation outputs.

The issues outlined in the previous paragraph make the development of efficient size-reduction-oriented optimization techniques a practical necessity. In many cases [33,34], miniaturization is achieved at the stage of antenna topology development, and further parameter tuning mainly aims at meeting the goals concerning the electrical/field performance figures. However, explicit size reduction, with minimization of the antenna footprint being the primary goal, is more efficient in most cases [35]. When doing so, implicit treatment of design constraints (e.g., using a penalty functions approach [34]) is a convenient strategy. In this context, several attempts have been made to facilitate the exploration of the feasible region boundary [35–37], which is an important aspect of the miniaturization process because many constraints are active at the minimum-size design [35]. Regardless of these advancements, high cost of the optimization process remains the major bottleneck of EM-driven antenna optimization, including miniaturization-oriented schemes. It may be an issue even for local search routines (gradient-based [38], or derivative free [39]), let alone global procedures, especially when using population-based nature-inspired methods [40–44]. The literature offers a number of techniques developed to improve the computational efficiency of the optimization processes. These include utilization of adjoint sensitivities [45,46], sparse sensitivity updates [47,48], as well as a growing class of surrogate-assisted frameworks [49]. The latter can employ either physics-based [50] or approximation (data-driven) surrogates [51]. Physics-based models incorporate the problem-specific knowledge encoded into the underlying low-fidelity representation of the antenna at hand. Upon suitable correction, the low-fidelity model can be used as a reliable prediction tool guiding the search process towards the optimum design. The popular procedures capitalizing on this concept include space mapping [52], cognition-driven design [53], response correction [54,55], or feature-based optimization [56]. The downside of physics-based surrogates is a relatively high cost of evaluating the low-fidelity model, which—in the case of antennas—is typically based on coarse-discretization EM simulations [57]. Approximation surrogates are considerably more popular due to their versatility, easy handling, as well as lower evaluation cost. There is an abundance of practical techniques available, including kriging [58], radial basis functions [59], neural networks [60], polynomial chaos expansion [61], or support vector regression [62]. Data-driven models can either entirely replace EM simulations [63], or be iteratively refined in the course of the

optimization process using sequential sampling methods [64]. Unfortunately, this class of models also suffers from certain deficiencies, especially in the context of antenna design, primarily related to the curse of dimensionality [65], but also high nonlinearity of antenna responses which are challenging to model.

When it comes to size reduction, the major role is played by local algorithms, which is because the early stages of antenna development typically yield reasonable initial designs, and global search is most often unnecessary. Available methods of expediting gradient-based procedures such as adjoint sensitivities [66], or sparse sensitivity updates [67], have been outlined before. The latter group is more generic because of not being intrusive (from the perspective of the EM simulation software); specific acceleration mechanisms such as adaptive Broyden updates [47] or Jacobian change tracking [48], offer computational savings of up to sixty percent as compared to the conventional methods with minor degradation of the design quality [47,67]. Variable-fidelity techniques with a notable example of space mapping [49], or response correction routines [68], can be even more efficient; however, the management of model fidelity is far from trivial [69].

This paper proposes an algorithmic framework for reduced-cost size reduction of antenna structures. Our approach involves multi-fidelity EM simulation models incorporated into a trust-region gradient-based procedure, as well as an appropriate formulation of the design task that allows for efficient handling of design constraints while explicitly targeting miniaturization of the antenna footprint. The computational model fidelity is governed by the convergence status of the algorithm, with the lowest usable discretization density utilized in the early stages, and the high-fidelity representation employed towards the end of the process. This ensures considerable computational savings while retaining acceptable reliability of the process. Furthermore, there is no need for sophisticated model management procedures. For demonstration purposes, the presented framework is applied to size reduction of two broadband antennas, and benchmarked against the reference trust-region algorithm. The obtained reduction of the computational cost is almost eighty percent without quality degradation.

2. Optimization-Based Antenna Miniaturization with Multi-Fidelity Simulations

This section introduces the proposed multi-fidelity framework for optimization-based miniaturization of antenna structures. We start by formulating the size-reduction problem as a constrained optimization task (Section 2.1), followed by a brief description of the trust-region gradient-based algorithm utilized as the main optimization engine (Section 2.2). Multi-fidelity models in the context of design optimization are discussed in Section 2.3. Section 2.4 provides the details concerning our multi-fidelity optimization procedure.

2.1. Optimization-Based Size Reduction. Problem Formulation

As explained in the introduction, numerical optimization has become ubiquitous in the development of antenna structures, especially in the later stages of the design process that require meticulous adjustment of geometry parameters. The latter is instrumental in boosting the performance figures as much as possible in order to meet the specifications imposed thereon. One of such objectives is a reduction of the antenna size, which is a prerequisite in many modern applications, e.g., wireless sensing, 5G communications, or IoT, to name just a few. In general, finding a minimum-size design is a multi-criterial problem because—apart from antenna dimensions—one has to account for performance requirements imposed on the impedance bandwidth, and, perhaps, other responses (axial ratio bandwidth, gain variability, etc.).

For the purpose of this work, we consider size reduction from the perspective of single-objective design, where all other requirements are handled by means of appropriately defined constraints. By denoting the vector of adjustable antenna parameters as x , the optimization problem can be formulated as:

$$x^* = \operatorname{argmin}_x U(x) \quad (1)$$

subject to $g_k(\mathbf{x}) \leq 0, k = 1, \dots, n_g$, and $h_k(\mathbf{x}) = 0, k = 1, \dots, n_h$ (inequality and equality constraints, respectively). The objective (or merit) function U quantifies the quality of the design. Because we are concerned with antenna miniaturization, the fundamental form of U will be $U(\mathbf{x}) = A(\mathbf{x})$, where A is the footprint area of the structure (in the case of microstrip antennas) or any other relevant measure of the antenna size (e.g., the volume for DRA devices).

In antenna design, the constraints are typically in the form of the acceptance thresholds for specific responses. The requirements imposed on antenna characteristics can be categorized as expensive ones, because their evaluation requires EM analysis. In this case, it is more convenient to handle them implicitly, using a penalty function approach [70], i.e., through an appropriate modification of the cost function U , where the primary objective is supplemented by additional terms that quantify possible constraint violations. Consequently, the design problem is reformulated into:

$$\mathbf{x}^* = \underset{\mathbf{x}}{\operatorname{argmin}} U_P(\mathbf{x}) \quad (2)$$

where the function U_P is of the form:

$$U_P(\mathbf{x}) = U(\mathbf{x}) + \sum_{k=1}^{n_g+n_h} \beta_k c_k(\mathbf{x}) \quad (3)$$

The penalty functions $c_k(\mathbf{x})$ measure violations of the respective requirements; β_k are the penalty coefficients. For the sake of clarity, below, we provide a few examples of constraints and the corresponding penalty functions:

- Ensuring that the antenna reflection $S_{11}(\mathbf{x}, f)$ does not exceed -10 dB within the operating frequency range F , i.e., $|S_{11}(\mathbf{x}, f)| \leq -10$ dB for $f \in F$. The penalty function can be of a form $c(\mathbf{x}) = [(\max\{S(\mathbf{x}) + 10, 0\})/10]^2$, where $S(\mathbf{x}) = \max\{f \in F: |S_{11}(\mathbf{x}, f)|\}$. Here, the utilization of the second power ensures smoothness of U_P at the feasible region boundary. The latter is important as most constraints are active at the optimum design. In general, adjusting the power factor allows for controlling the constraint 'hardness'; the second power provides a certain leeway for small violations.
- Ensuring that the axial ratio $AR(\mathbf{x}, f)$ of a CP antenna does not exceed 3 dB within the operating range F , i.e., $AR(\mathbf{x}, f) \leq 3$ dB for $f \in F$. The penalty function can be of a form $c(\mathbf{x}) = [(\max\{A_R(\mathbf{x}) - 3, 0\})/3]^2$, where $A_R(\mathbf{x}) = \max\{f \in F: AR(\mathbf{x}, f)\}$.

Ensuring that variability of realized gain $G(\mathbf{x}, f)$ does not exceed 2 dB within the frequency range of interest F , i.e., $\Delta G(\mathbf{x}, f) \leq 2$ dB for $f \in F$. In this case, we would have $c(\mathbf{x}) = [(\max\{G(\mathbf{x}) - 3, 0\})/3]^2$, where $G(\mathbf{x}) = \max\{f \in F: \Delta G(\mathbf{x}, f)\}$.

2.2. Reference Algorithm: Trust-Region Gradient-Based Procedure

The core procedure for a multi-fidelity size reduction procedure presented in this paper is the standard trust-region (TR) algorithm [71]. Its formulation is briefly recalled below. It will also be used in Section 3 as a benchmark with respect to which we determine the computational savings obtained by our method.

The TR algorithm is an iterative procedure that solves the task (2) by generating a sequence of approximations $\mathbf{x}^{(i)}, i = 0, 1, \dots$, to \mathbf{x}^* ($\mathbf{x}^{(0)}$ being the initial design). These are obtained by constrained optimization carried out at the level of a local model $U_L^{(i)}$ of the relevant antenna responses, typically the first-order Taylor expansions established at the current design $\mathbf{x}^{(i)}$. For a reflection response, we have

$$S_L^{(i)}(\mathbf{x}, f) = S_{11}(\mathbf{x}^{(i)}, f) + \mathbf{G}_S(\mathbf{x}^{(i)}, f) \cdot (\mathbf{x} - \mathbf{x}^{(i)}) \quad (4)$$

In (4), the symbol $\mathbf{G}_S(\mathbf{x}^{(i)}, f)$ stands for the gradient of antenna reflection characteristic at the design $\mathbf{x}^{(i)}$ and frequency f . Because our primary objective is size reduction, it is not necessary to use any approximation to represent the footprint area $A(\mathbf{x})$, which can be directly calculated from the parameter vector \mathbf{x} . However, when evaluating the constraints,

the linear model $U_L^{(i)}$ is employed instead of the corresponding characteristic (e.g., with $S_L^{(i)}(\mathbf{x})$ replacing S_{11} , and, similarly, for other types of responses, such as gain or axial ratio).

The iteration point $\mathbf{x}^{(i+1)}$ is obtained as:

$$\mathbf{x}^{(i+1)} = \arg \min_{\mathbf{x}; -\mathbf{d}^{(i)} \leq \mathbf{x} - \mathbf{x}^{(i)} \leq \mathbf{d}^{(i)}} U_L^{(i)}(\mathbf{x}) \quad (5)$$

Note that the optimization process (5) is conducted within an interval $\mathbf{x}^{(i)} - \mathbf{d}^{(i)} \leq \mathbf{x} \leq \mathbf{x}^{(i)} + \mathbf{d}^{(i)}$ (inequalities are understood component-wise), which serves as the trust region. The TR size vector is proportional to the parameter ranges to avoid variable scaling [47]. The new point $\mathbf{x}^{(i+1)}$ is accepted if and only if $U_P(\mathbf{x}^{(i+1)}) < U_P(\mathbf{x}^{(i)})$, i.e., the improvement of the objective function is observed. Otherwise, the vector $\mathbf{d}^{(i)}$ is reduced [48], and the iteration is restarted from $\mathbf{x}^{(i)}$. Reliable predictions, i.e., with high values of the gain ratio $(U_P(\mathbf{x}^{(i+1)}) - U_P(\mathbf{x}^{(i)})) / (U_L^{(i)}(\mathbf{x}^{(i+1)}) - U_L^{(i)}(\mathbf{x}^{(i)})) > 0.75$ lead to the increase of the size vector [48]. The gradients of antenna responses are estimated using finite differentiation. For n adjustable parameters, this entails n additional EM evaluations of the structure per iteration.

2.3. Multi-Fidelity Simulation Models

In this work, we aim at accelerating the EM-driven size reduction process of antennas by employing multi-fidelity simulation models. Although variable-fidelity methods have been around for about two decades or so, they were mostly restricted to two model resolutions, conventionally referred to as coarse (or low-fidelity) and fine (or high-fidelity). In some areas, especially microwave engineering, lower fidelity models are often implemented using circuit theory (equivalent networks [52]), whereas in the realm of antenna design, these are typically coarse-discretization EM simulations [50]. More information about possible categories of coarse models can be found in [54]. A typical arrangement is to use an appropriately corrected coarse model as a (usually local) replacement of the high-fidelity simulation (e.g., space mapping [49], manifold mapping [72]). Other options include machine learning methods with the lower fidelity model involved in the initial parameter space exploration [73], or two-level surrogate modelling approaches (co-kriging [74], two-stage Gaussian process regression [75]). A common inconvenience is that the low-fidelity model setup (its resolution versus evaluation time) may be critical to the performance of whatever algorithm it is applied in [70].

As opposed to what was outlined above, here, the goal is to utilize and control the entire range of EM models of different fidelities using an appropriate model management scheme. Consider Figure 1 showing an example of a compact monopole antenna as well as several of its reflection responses corresponding to different discretization densities of the structure parameterized by means of LPW (lines per wavelength), which is a standard way of controlling the mesh density in CST Microwave Studio. The evaluation accuracy can be traded off for a shorter simulation time. Beyond a certain limit, the model is no longer usable because its reliability becomes questionable. Also, lowering the model fidelity increases the level of numerical noise, which makes sensitivity estimation by means of finite differentiation prone to errors.

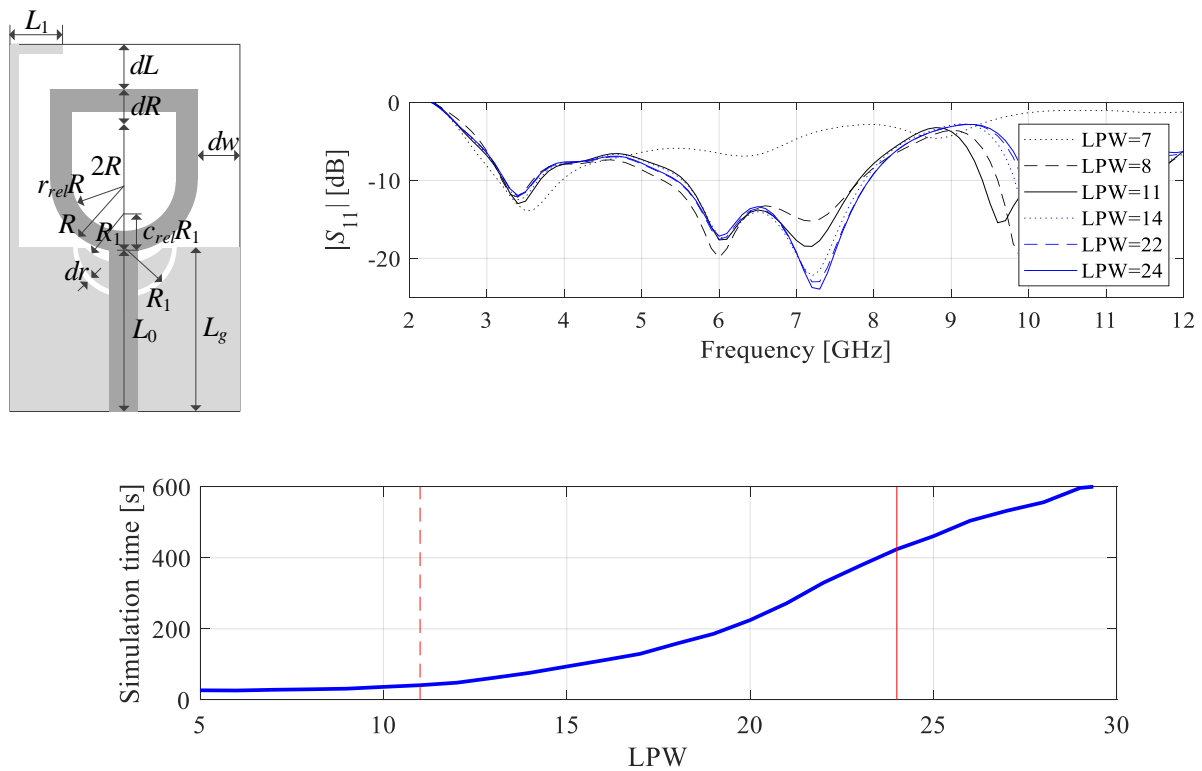


Figure 1. Multi-fidelity simulation models for an exemplary broadband monopole antenna [76]. The picture shows the antenna geometry, the family of reflection characteristics for several discretization densities of the structure (controlled using the lines-per-wavelength parameter LPW), and the simulation time versus LPW (averaged over several antenna geometries). The mesh densities corresponding to the high-fidelity model and the lowest usable low-fidelity one are marked using the vertical lines, solid and dashed, respectively.

Through investigating the data shown in Figure 1, a designer can establish two boundary discretization levels, one corresponding to the lowest LPW that is of practical utility (marked as L_{\min}), and another one for the high-fidelity model (marked as L_{\max}). The latter corresponds to the level of accuracy that is considered sufficient for design purposes. The algorithm proposed in this work employs the simulation models within the entire range of discretization densities $L_{\min} \leq L \leq L_{\max}$. The model management strategy is developed by taking into account several assumptions that aim at improving the computational efficiency of the optimization process while maintaining reliability.

2.4. Model Management Scheme

Our goal is to incorporate multi-fidelity simulation models into the trust-region algorithm of Section 2.2, utilized as the core optimization procedure, with the intention of achieving computational benefits, and to maintain the reliability of the design process. Section 2.3 explained the procedure of determining the range of discretization levels L for the considered antenna structure, starting from the lowest usable resolution L_{\min} to the high-fidelity representation L_{\max} . The model management strategy is developed by taking into account the following factors:

- To enable a reduction of the computational cost of the algorithm, the optimization process should be initiated with the lowest-fidelity model;
- To ensure reliability of the process, the final stages of the algorithm should involve the high-fidelity model;
- The transition towards higher-fidelity models should be gradual and governed by the reliable factors that determine the optimization status, in particular the expected distance from the optimum. Here, we use the convergence status, measured by the

- distance between two subsequent iteration points $\|x^{(i+1)} - x^{(i)}\|$ (convergence in argument), but also the improvement of the objective function value $U_P(x^{(i+1)}) - U_P(x^{(i)})$; reduction of both indicates that the optimization process is getting closer to termination;
- In order to facilitate the stability of the optimization process, the transition between the models of various fidelities should be possibly smooth with respect to the factors mentioned above.

The termination criterion for the algorithm is based on the logical alternative of the conditions $\|x^{(i+1)} - x^{(i)}\| < \epsilon_x$ (convergence in argument), $\|d^{(i)}\| < \epsilon_x$ (reduction of the trust region), or $|U_P(x^{(i+1)}) - U_P(x^{(i)})| < \epsilon_U$ (convergence in objective function value) with user-defined thresholds ϵ_x and ϵ_U (both set to 10^{-3} in the numerical experiments of Section 3). Our management scheme is based on an auxiliary parameter:

$$Q^{(i)}(\epsilon_x, \epsilon_U) = \max \left\{ \frac{\epsilon_x}{\|x^{(i+1)} - x^{(i)}\|}, \frac{\epsilon_U}{|U_P(x^{(i+1)}) - U_P(x^{(i)})|} \right\} \tag{6}$$

which is used to adjust the discretization density parameter $L(i)$ at the i -th iteration of the optimization algorithm according to the formula:

$$L^{(i+1)} = \begin{cases} L_{\min} & \text{if } Q^{(i)}(\epsilon_x, \epsilon_U) \leq M \\ \max \left\{ L^{(i)}, L_{\min} + (L_{\max} - L_{\min}) \left[Q^{(i)}(\epsilon_x, \epsilon_U) - M \right]^{\frac{1}{\alpha}} \right\} & \text{otherwise} \end{cases} \tag{7}$$

It can be observed that (7) enforces monotonicity of the model discretization density as a function of the iteration index. The coefficient M (set to 10^{-2} in Section 3) is used to decide how far from the algorithm convergence we intend to initiate the process of increasing the model fidelity, whereas α (set to 3 in Section 3) determines the shape of the discretization profile. For the listed values, the parameter L begins to grow when the $Q^{(i)}$ is two decades away from convergence; also the initial increase is relatively fast. Having in mind the typical dependence between L and the evaluation time, this sort of setup leads to accuracy improvements without significant CPU costs. The discretization level profiles for selected values of the control parameter α have been shown in Figure 2.

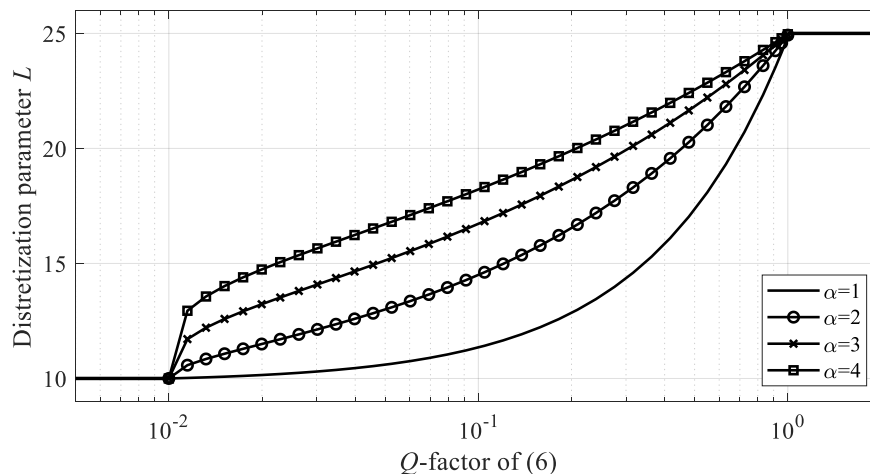


Figure 2. Illustration of discretization level profiles generated by Equation (7), parameterized by the control parameter α . For demonstration purposes, the following setup was used: $L_{\min} = 10$, $L_{\max} = 25$, and $M = 10^{-2}$.

A potential deficiency of the scheme (7) is that $L^{(i)}$ may never actually reach L_{\max} . A possible scenario is when some of algorithm iterations are unsuccessful and the algorithm terminates upon one or more consecutive reductions of the trust region size vector d .

Having this in mind, an additional procedure is implemented, which enforces utilization of the high-fidelity model at the last stage of the optimization process (in case it has not been already employed). Upon algorithm termination, the following operation is performed:

$$\text{IF } L^{(i)} < L_{\max} \text{ THEN } L^{(i+1)} = L_{\max} \text{ AND } \mathbf{d}^{(i+1)} = M_d \mathbf{d}^{(i)} \frac{\varepsilon_x}{\|\mathbf{d}^{(i)}\|} \quad (8)$$

where the multiplication factor M_d (set to 10 in Section 3) is introduced to create a room for design improvement upon switching to L_{\max} . If (8) is executed, the termination condition is bypassed, and additional iterations may be carried out with $L = L_{\max}$. As mentioned before, this is only activated if L was below L_{\max} during the normal algorithm run.

The final acceleration mechanism is to evaluate the antenna response gradients at the lower-fidelity level than the antenna response itself. When operating with the discretization level $L^{(i)}$, the sensitivities are estimated by finite differentiation at the level:

$$L_{FD} = \max\{L_{\min}, \lambda L^{(i)}\} \quad (9)$$

with $0 \leq \lambda \leq 1$ (another control parameter, set to $\lambda = 2/3$ in Section 3). This mechanism capitalizes on the observation that despite of certain misalignment of the models of different fidelities, their correlation (i.e., responses change in a similar manner upon corresponding alterations of geometry parameters) is normally well preserved. This is sufficient to yield a reliable representation of the gradients, provided that the coefficient λ is not excessively small.

2.5. Optimization Algorithm

The proposed multi-fidelity optimization algorithm combines the TR procedure outlined in Section 2.2, and the model management strategy described in Section 2.4. The control parameters were mentioned before but they are gathered again below for the sake of the reader's convenience:

- $\varepsilon_x, \varepsilon_U$ —algorithm termination thresholds, decided upon based on the required resolution of the optimization procedure (Section 2.4);
- M —threshold for initiating discretization level increase (Section 2.4);
- α —shape parameter of the discretization level profile (Section 2.4);
- λ —parameter for setting discretization level L_{FD} for sensitivity estimation, cf. (10);
- M_d —trust-region size multiplication factor (cf. (8)).

The lowest and the highest fidelity levels L_{\min} and L_{\max} (cf. Section 2.3) are determined through the grid convergence study. In particular, L_{\max} is usually established as the discretization level the increase of which does not lead to meaningful changes of the antenna characteristics, whereas L_{\min} corresponds to the coarsest discretization for which the simulated responses still properly account for the relevant features (e.g., resonances, etc.).

Figure 3 summarizes the operation of the algorithm in the form of a pseudocode. Therein, the relevant antenna characteristics are represented as $\mathbf{R}(x)$; the symbol $J_R(x)$ stand for the response sensitivity matrix, both at the design x . The initial design is denoted as $x^{(0)}$. Figure 4 shows the flow diagram of the algorithm.

1. Set the iteration counter $i = 0$, and $L^{(i)} = L_{\min}$;
2. Evaluate antenna response $\mathbf{R}(\mathbf{x}^{(i)})$ at the discretization level $L^{(i)}$;
3. Evaluate antenna sensitivities $\mathbf{J}_R(\mathbf{x}^{(i)})$ at the discretization level L_{FD} (cf. (9));
4. Construct a linear model $\mathbf{L}^{(i)}(\mathbf{x}) = \mathbf{R}(\mathbf{x}^{(i)}) + \mathbf{J}_R(\mathbf{x}^{(i)}) \cdot (\mathbf{x} - \mathbf{x}^{(i)})$;
5. Obtain the design $\mathbf{x}^{(i+1)}$ by solving (5);
6. Evaluate antenna response $\mathbf{R}(\mathbf{x}^{(i+1)})$ at the discretization level $L^{(i)}$;
7. Update trust-region size vector $\mathbf{d}^{(i)}$ [58];
8. **if** $U_P(\mathbf{x}^{(i+1)}) < U_P(\mathbf{x}^{(i)})$
 Compute $L^{(i+1)}$ using (7);
 Set $i = i + 1$;
 end
9. **if** $\|\mathbf{x}^{(i+1)} - \mathbf{x}^{(i)}\| < \varepsilon_x$ **OR** $\|\mathbf{d}^{(i)}\| < \varepsilon_x$ **OR** $|U_P(\mathbf{x}^{(i+1)}) - U_P(\mathbf{x}^{(i)})| < \varepsilon_U$
 if $L^{(i)} < L_{\max}$
 Set $L^{(i)} = L_{\max}$ and modify $\mathbf{d}^{(i)}$ according to (8); go to 3;
 else
 Go to 10;
 end
- else**
 Go to 3;
 end
10. END.

Figure 3. EM-driven size reduction using multi-fidelity simulations: operational flow. In the presented pseudocode, the relevant antenna responses (EM-simulated at the design \mathbf{x}) are denoted as $\mathbf{R}(\mathbf{x})$; $\mathbf{J}_R(\mathbf{x})$ stand for the sensitivity matrix, also at the design \mathbf{x} .

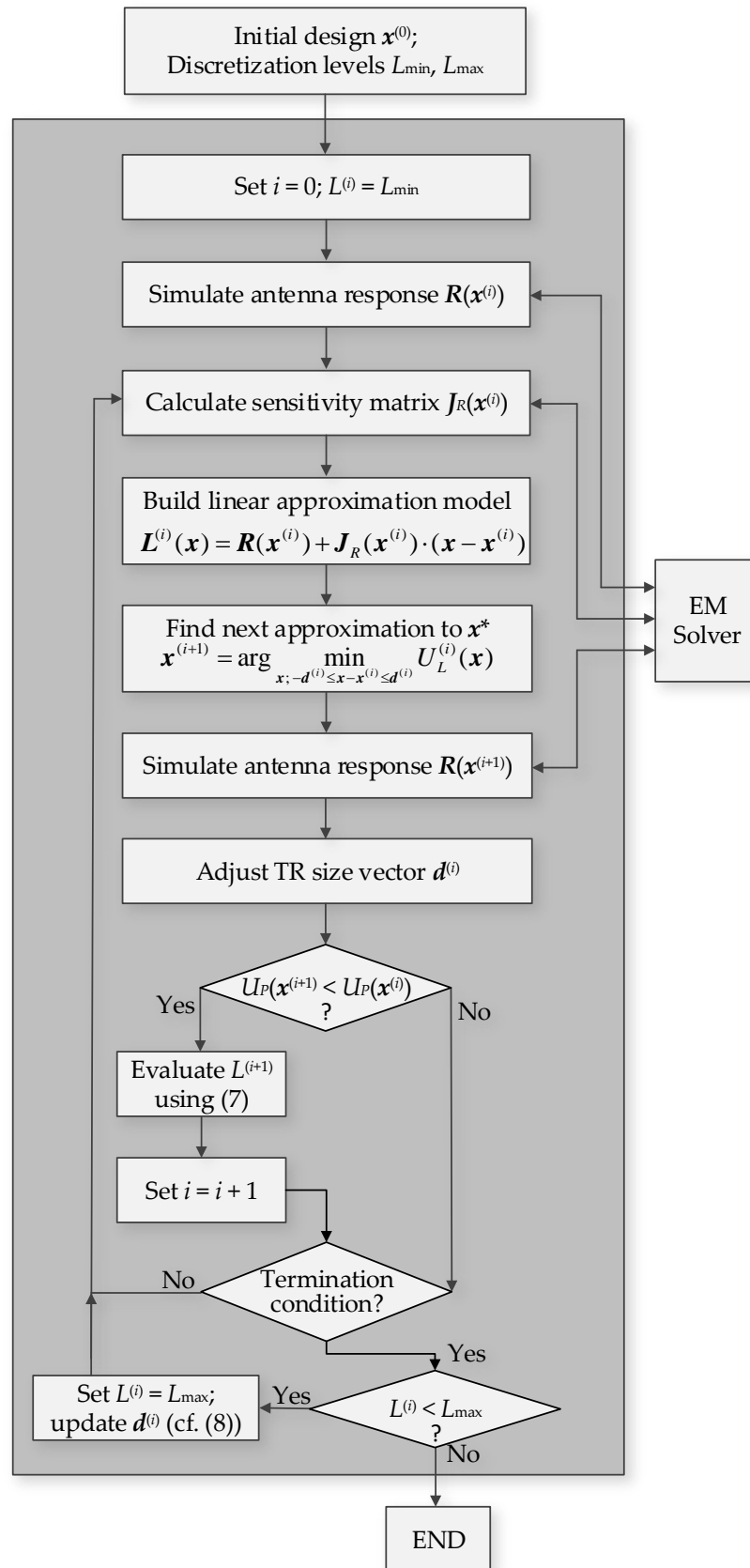


Figure 4. EM- driven size-reduction using multi-fidelity simulations: flow diagram.

3. Demonstration Case Studies and Benchmarking

In this section, the multi-fidelity optimization framework described in Section 2 is validated using two examples of miniaturized broadband microstrip antennas. In both cases, the objective is to reduce the antenna footprint while maintaining a sufficient reflection level across the operating band of the structure. The main goal of the numerical experiments is to identify possible computational savings with respect to the conventional trust-region algorithm (cf. Section 2.2), as well as to verify whether the improved efficiency is associated with design quality degradation. The experimental validation of the designs of the presented benchmark antennas has not been provided as they are not entirely relevant to the topic of the paper. Furthermore, all of the considered structures have been already validated not only in the respective source papers [77,78], but also in the papers regarding their numerical optimization (e.g., [47,76]). Thus, the results provided in the manuscript are sufficient to substantiate the inferred conclusions, especially given the scope of this work, which, is the development of a novel optimization framework rather than novel antenna structures.

3.1. Benchmark Antennas

Consider the ultra-wideband microstrip monopole antennas shows in Figure 5. Relevant information concerning both structures have been gathered in Table 1. The computational models are implemented in CST Microwave Studio and evaluated using the time-domain solver. The models incorporate the SMA connectors.

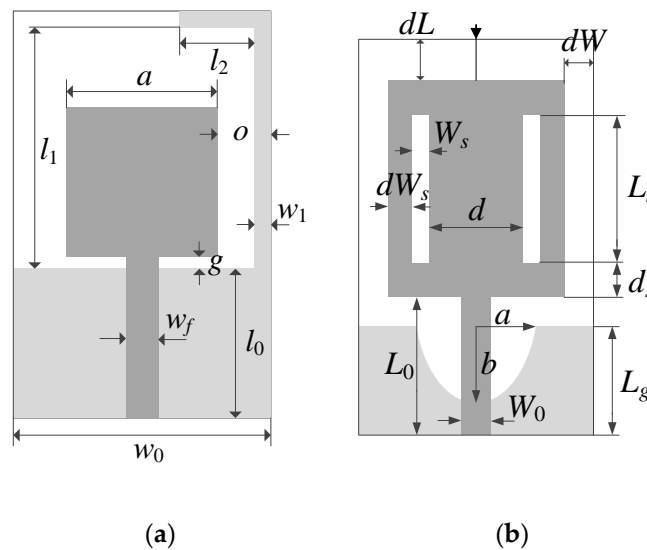


Figure 5. Benchmark monopole antennas: (a) Antenna I, (b) Antenna II. The feeding line and the radiator marked using the dark gray shade; ground plane marked using light gray shade.

Table 1. Benchmark Monopole Antennas.

Antenna	Substrate	Designable Parameters (mm)	Other Parameters (mm)
I [77]	RF-35 ($\epsilon_r = 3.5, h = 0.762$ mm)	$x = [l_0 \ g \ a \ l_1 \ l_2 \ w_1 \ o]^T$	$w_0 = 2o + a, w_f = 1.7$
II [78]	FR4 ($\epsilon_r = 4.3, h = 1.55$ mm)	$x = [L_g \ L_0 \ L_s \ W_s \ d \ dL \ d_s \ dW_s \ dW \ a \ b]^T$	$W_0 = 3.0$

Information about the considered ranges of structure discretization densities parameterized by the lines-per-wavelength (LPW) can be found in Table 2, which specifies the lowest value L_{\min} , as well as the value L_{\max} corresponding to the high-fidelity model (cf. Section 2.3). The table also provides the simulation times at both L_{\min} and L_{\max} . Observe, that the simulation times reported in Table 2 were provided merely in order to

provide information on the time evaluation ratio between the high-fidelity model and the lowest-fidelity one, which is important from the point of view of the expected speedup.

Table 2. Benchmark Monopole Antennas: Discretization Density Ranges and Simulation Times.

Antenna	Lowest-Fidelity Model		High-Fidelity Model	
	L_{\min}	Simulation Time [s]	L_{\max}	Simulation Time [s]
I	10	42	21	150
II	10	46	20	265

A graphical illustration of the dependence between LPW and the simulation time can be found in Figure 6. The time evaluation ratio between the structure discretized at L_{\max} (high-fidelity model) and L_{\min} (lowest fidelity model) is slightly less than four for Antenna I, and almost six for Antenna II. This indicates that the proposed optimization framework may indeed enable considerable CPU savings, as most of the operations are carried out at the lower-fidelity simulation levels. Both antenna structures are to operate in UWB frequency range from 3.1 GHz to 10.6 GHz. The primary objective is a reduction of the antenna footprint $A(x)$, defined as the area of the dielectric substrate. Miniaturization is subject to a reflection constraint $|S_{11}(x,f)| \leq -10$ dB, and the objective function is defined as in (3), using the penalty function approach.

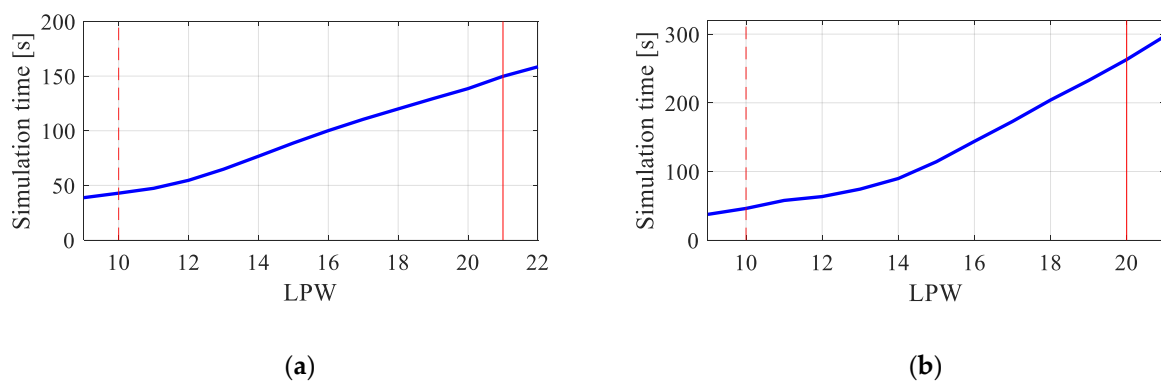


Figure 6. Benchmark monopole antennas: simulation time versus fidelity level: (a) Antenna I, (b) Antenna II. Discretization density parameters (lines-per-wavelength, LPW) for the minimum (---) and the maximum (—) considered level of fidelity (vertical lines).

3.2. Experimental Setup

For the purpose of validating the proposed multi-fidelity algorithm, the benchmark antennas were optimized ten times starting from random initial designs. The reason is to account for a multimodality of the considered structures. Miniaturized antennas normally feature a certain redundancy of parameters due to the topological alterations introduced as a way of achieving more compact geometries. This normally leads to complex relationships between the adjustable parameters of the antenna and its characteristics. One of the results is the presence of multiple local optima. Because the considered routines (both the reference and the proposed procedure) are local, statistical investigations are necessary to obtain a meaningful evaluation of the algorithm performance. In particular, we compare the average performance as well as analyze the statistical indicators of the repeatability of solutions as described below. The following three criteria are considered:

- Computational cost of the optimization process expressed in terms of the equivalent number of high-fidelity EM simulations of the antenna structure at hand; in the case of multi-fidelity algorithm, the simulation times of the model at a given level of fidelity

are recalculated into the equivalent number of high-fidelity analyzes using the curves presented in Figure 6;

- Design quality measures as the average antenna footprint at the optimized design;
- Repeatability of results measures by means of the standard deviation of the obtained antenna footprint area. Clearly, the standard deviation will be positive even for the reference algorithm due to the aforementioned multimodality; consequently, the potential quality degradation should be considered as compared to the respective figures for the reference algorithm rather than to the zero value.

The values of the control parameters of the algorithm to be used in our experiments have been mentioned before but they are gathered again here for the convenience of the reader: $M = 10^{-2}$ (threshold to enable the discretization level increase; cf. Section 2.4), $\alpha = 3$ (control parameter for discretization level profile; cf. Section 2.4), $\lambda = 2/3$ (control parameter for setting discretization level L_{FD} for finite differentiation; cf. (10)), $M_d = 10$ (multiplication factor for increasing TR size in (8)). The termination thresholds are fixed at $\varepsilon_x = \varepsilon_U = 10^{-3}$ (cf. Section 2.4) and kept the same for the proposed algorithm and the benchmark.

3.3. Results and Discussion

The optimization results obtained by means of the proposed and the reference algorithms have been gathered in Tables 3 and 4 for Antenna I and II, respectively. The tables indicate the optimization cost expressed in terms of the equivalent number of high-fidelity antenna simulations, and averaged over ten independent runs, the computational savings achieved with the multi-fidelity algorithm (versus the reference), as well the aforementioned quality indicators. These include the average antenna footprint, the quality degradation w.r.t. to the reference, as well as the standard deviation of the antenna footprint (as the repeatability indicator). It should be reiterated that the running cost of the multi-fidelity algorithm is calculated based on the time evaluation curves of Figure 6. Figure 7 illustrates the antenna responses at the initial and optimized designs for the representative algorithm runs. It can be observed that the maximum in-band reflection at the optimum design is close to the acceptance threshold of -10 dB. On the one hand, it indicates that the assumed constraint handling approach works as expected. Slight violations are due to the fact that penalty function approach turns the constraint into the soft one, cf. Section 2.1. On the other hand, it corroborates the expectation that the reflection constraint is active at the optimum, i.e., further reduction of the antenna footprint in the vicinity of the optimum design would lead to constraint violation.

Table 3. Numerical Results for Antenna I.

Algorithm	Performance Figure				
	Cost ¹	Cost Savings ²	Footprint Area A (mm ²) ³	ΔA (mm ²) ⁴	Std(A) (mm ²) ⁵
Conventional TR search	106.8	-	308.2	-	37.2
Multi-fidelity (this work)	34.7	67.5%	310.5	2.3	41.3

¹ Number of equivalent high-fidelity EM simulations averaged over 10 algorithm runs. ² Relative computational savings in percent w.r.t. the reference algorithm. ³ Obtained footprint area, averaged over 10 algorithm runs. ⁴ Increase of the footprint area w.r.t. the reference algorithm, averaged over 10 algorithm runs. ⁵ Standard deviation of the footprint area across the set of 10 algorithm runs.

Table 4. Numerical Results for Antenna II.

Algorithm	Performance Figure				
	Cost ¹	Cost Savings ²	Footprint Area A (mm ²) ³	ΔA (mm ²) ⁴	Std(A) (mm ²) ⁵
Conventional TR search	164.9	-	212.8	-	14.2
Multi-fidelity (this work)	39.4	76.1%	209.1	-3.7	5.6

¹ Number of equivalent high-fidelity EM simulations averaged over 10 algorithm runs. ² Relative computational savings in percent w.r.t. the reference algorithm. ³ Obtained footprint area, averaged over 10 algorithm runs. ⁴ Increase of the footprint area w.r.t. the reference algorithm, averaged over 10 algorithm runs. ⁵ Standard deviation of the footprint area across the set of 10 algorithm runs.

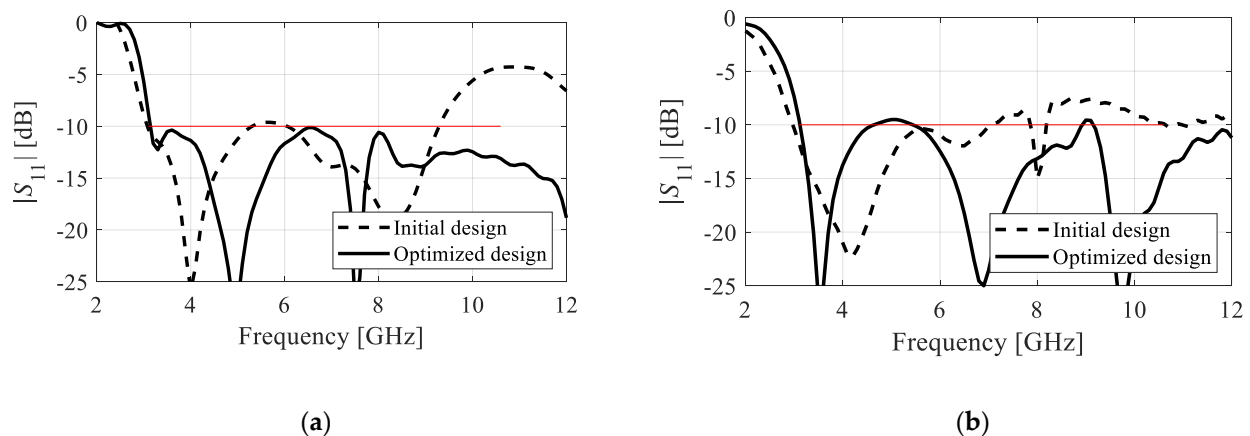


Figure 7. Reflection responses for the representative runs of the proposed multi-fidelity algorithm for simulation-driven size reduction: (a) Antenna I, (b) Antenna II. The initial and optimized designs are marked using the dashed and solid lines, respectively. The horizontal lines mark the design specifications. Note that the maximum reflection at the optimized design is around the level of -10 dB which indicates that the reflection constraint is active.

Based on the result analysis, one can conclude that the multi-fidelity algorithm enables significant computational savings, which are as high as 68 percent for Antenna I and 76 percent for Antenna II. In other words, the involvement of multi-fidelity simulations in the form proposed in this work speeds up the optimization process almost four times on the average.

At the same time, there is only slight, almost negligible, quality degradation for Antenna I, and quality improvement for Antenna II. Given very small differences of about three square millimeters, which is less than two percent of the average antenna footprint area, we can conclude that design quality is the same for both algorithms. The same can be said about the repeatability of results as the standard deviations are at similar levels for both algorithms. It can be noticed that the standard deviation is higher for Antenna I, which is mainly contributed by a poor quality of a typical initial design (in terms of exhibiting a high level of in-band reflection), which makes the optimization problem more challenging: at the initial stages of the algorithm run, the main effort is put in relocating the design into the feasible region of the parameter space.

Figure 8 shows the convergence plots and the changes of antenna discretization density parameter for the typical algorithm runs for both considered antennas. It can be observed that the first few iterations are executed with the lowest fidelity. The discretization density starts increasing as soon as the convergence factor $Q^{(i)}(\epsilon_x, \epsilon_U)$ falls below $M = 10^{-2}$ (cf. (6)), and is gradually increased afterwards. This allows for covering most of the distance from the starting point to the close vicinity of the optimum using the least expensive computational model and, hence, obtain considerable computational benefits.

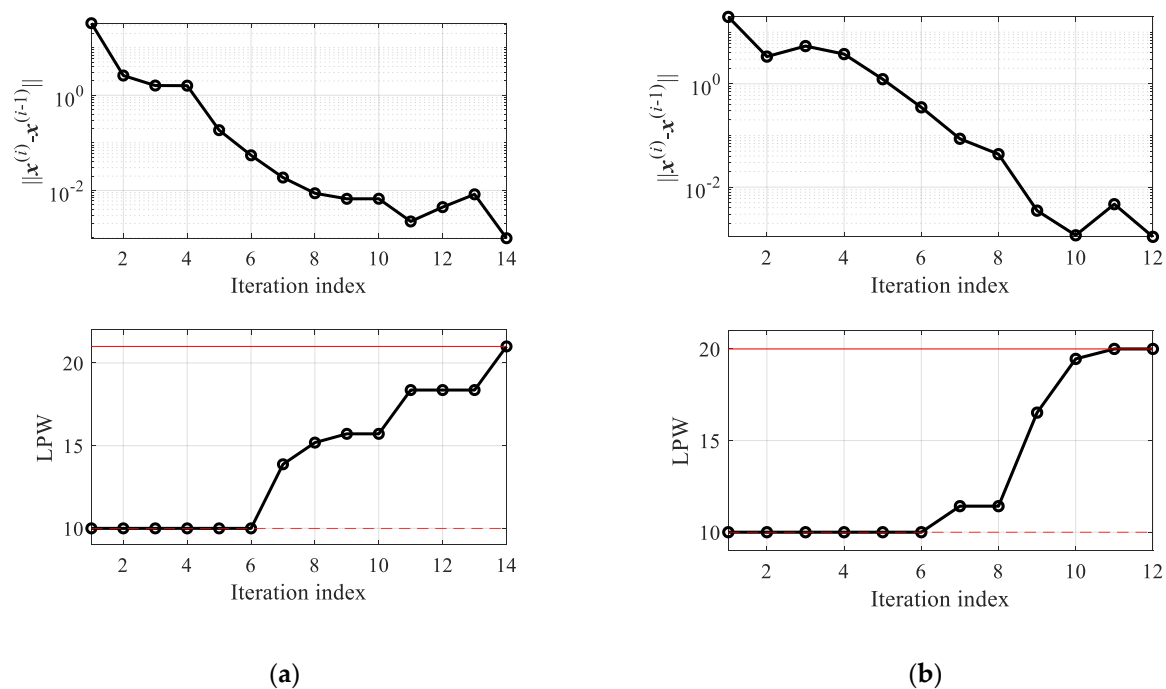


Figure 8. Convergence plots (top) and the evolution of antenna discretization density (bottom) in terms of lines-per-wavelength (LPW) parameters in typical runs of the proposed algorithm for (a) Antenna I, (b) Antenna II. Horizontal lines correspond to the lowest fidelity L_{\min} (---), and the high-fidelity model L_{\max} (—).

Finally, it should be mentioned that the optimization algorithm presented in this work uses the same sensitivity updating scheme as the reference algorithm, i.e., full finite differentiation in each of the algorithm iteration. This leaves room for further improvements by incorporating some of the recent acceleration mechanisms in the form of sparse Jacobian updates as proposed in [47] or [48].

4. Conclusions

In the paper, a novel procedure for EM-driven miniaturization of antenna structures has been proposed. Our methodology incorporates multi-fidelity simulation models into the trust-region gradient search algorithm. The optimization task is formulated as explicit size reduction problem with implicit handling of design constraints using the penalty function approach. The model management scheme developed to control the antenna discretization density is based on the convergence status of the optimization process with the lowest fidelity (and the cheapest) model employed in the initial stages, and the model resolution gradually increased toward the conclusion of the algorithm run. The high-fidelity model is only used at the final stages. The proposed strategy enables a considerable speedup in comparison to the reference optimization procedure. The computational benefits are achieved without noticeable quality degradation. Numerical verification has been carried out using two broadband microstrip antennas optimized for minimum size, with the constraint imposed on the reflection characteristics. Statistical analysis of the results obtained for ten independent runs starting from random initial designs indicates that the average computational savings exceed seventy percent, and repeatability of solutions is as good as for the algorithm utilizing high-fidelity model only. The presented framework constitutes an attractive alternative to conventional method of optimization-based size reduction. It is generic and straightforward to apply as it does not involve any sophisticated methods for low-fidelity model correction. The future developments of this approach will aim at further improvement of computational efficiency by incorporating acceleration mechanisms at the stage of sensitivity updates.

Author Contributions: Conceptualization, S.K. and A.P.-D.; methodology, S.K. and A.P.-D.; software, S.K. and A.P.-D.; validation, S.K. and A.P.-D.; formal analysis, S.K.; investigation, S.K. and A.P.-D.; resources, S.K.; data curation, S.K. and A.P.-D.; writing—original draft preparation, S.K. and A.P.-D.; writing—review and editing, S.K.; visualization, S.K. and A.P.-D.; supervision, S.K.; project administration, S.K.; funding acquisition, S.K. All authors have read and agreed to the published version of the manuscript.

Funding: This work was supported in part by the Icelandic Centre for Research (RANNIS) Grant 206606, and by National Science Centre of Poland Grant 2017/27/B/ST7/00563.

Acknowledgments: The authors thank Dassault Systemes, France, for making CST Microwave Studio available.

Conflicts of Interest: The authors declare no conflict of interest. The funders had no role in the design of the study; in the collection, analyses, or interpretation of data; in the writing of the manuscript, or in the decision to publish the results.

References

1. Yang, Y.; Sun, B.; Guo, J. A low-cost, single-layer, dual circularly polarized antenna for millimeter-wave applications. *IEEE Ant. Wirel. Prop. Lett.* **2019**, *184*, 651–655. [[CrossRef](#)]
2. Bilgic, M.M.; Yegin, K. Modified annular ring antenna for GPS and SDARS automotive applications. *IEEE Ant. Wirel. Prop. Lett.* **2016**, *15*, 1442–1445. [[CrossRef](#)]
3. Mobashsher, A.T.; Pretorius, A.J.; Abbosh, A.M. Low-profile vertical polarized slotted antenna for on-road RFID-enabled intelligent parking. *IEEE Trans. Ant. Propag.* **2020**, *68*, 527–532. [[CrossRef](#)]
4. Qian, J.; Chen, F.; Xiang, K.; Chu, Q. Resonator-loaded multi-band microstrip slot antennas with bidirectional radiation patterns. *IEEE Trans. Ant. Propag.* **2019**, *67*, 6661–6666. [[CrossRef](#)]
5. Liu, J.; Su, T.; Liu, Z. High-gain grating antenna with surface wave launcher array. *IEEE Ant. Wirel. Prop. Lett.* **2018**, *17*, 706–709. [[CrossRef](#)]
6. Huang, H.; Gao, S.; Lin, S.; Ge, L. A wideband water patch antenna with polarization diversity. *IEEE Ant. Wirel. Prop. Lett.* **2020**, *19*, 1113–1117. [[CrossRef](#)]
7. Yang, X.; Ge, L.; Ji, Y.; Zeng, X.; Luk, K.M. Design of low-profile multi-band half-mode substrate-integrated waveguide antennas. *IEEE Trans. Ant. Propag.* **2019**, *67*, 6639–6644. [[CrossRef](#)]
8. Yang, H.; Fan, Y.; Liu, X. A compact dual-band stacked patch antenna with dual circular polarizations for BeiDou navigation satellite systems. *IEEE Ant. Wirel. Prop. Lett.* **2019**, *18*, 1472–1476. [[CrossRef](#)]
9. Jha, K.R.; Bukhari, B.; Singh, C.; Mishra, G.; Sharma, S.K. Compact planar multistandard MIMO antenna for IoT applications. *IEEE Trans. Ant. Propag.* **2018**, *66*, 3327–3336. [[CrossRef](#)]
10. Xue, K.; Yang, D.; Guo, C.; Zhai, H.; Li, H.; Zeng, Y. A dual-polarized filtering base-station antenna with compact size for 5G applications. *IEEE Ant. Wirel. Prop. Lett.* **2020**, *19*, 1316–1320. [[CrossRef](#)]
11. Agneessens, S.; Lemey, S.; Vervust, T.; Rogier, H. Wearable, small, and robust: The circular quarter-mode textile antenna. *IEEE Ant. Wirel. Prop. Lett.* **2015**, *14*, 1482–1485. [[CrossRef](#)]
12. Alqadami, A.S.M.; Nguyen-Trong, N.; Mohammed, B.; Stancombe, A.E.; Heitzmann, M.T.; Abbosh, A. Compact unidirectional conformal antenna based on flexible high-permittivity custom-made substrate for wearable wideband electromagnetic head imaging system. *IEEE Trans. Ant. Propag.* **2020**, *68*, 183–194. [[CrossRef](#)]
13. Pandit, S.; Mohan, A.; Ray, P. Compact frequency-reconfigurable MIMO antenna for microwave sensing applications in WLAN and WiMAX frequency bands. *IEEE Sens. Lett.* **2008**, *2*, 1–4. [[CrossRef](#)]
14. Pires, N.; Parra, T.; Skrivervik, A.K.; Moreira, A.A. Design and measurement of a differential printed antenna for a wireless sensor network node. *IEEE Ant. Wirel. Prop. Lett.* **2017**, *16*, 2228–2231. [[CrossRef](#)]
15. Roshna, T.K.; Deepak, U.; Sajitha, V.R.; Vasudevan, K.; Mohanan, P. A compact UWB MIMO antenna with reflector to enhance isolation. *IEEE Trans. Ant. Propag.* **2015**, *63*, 1873–1877. [[CrossRef](#)]
16. Koziel, S.; Cheng, Q.S.; Li, S. Optimization-driven antenna design framework with multiple performance constraints. *Int. J. RF Microw. CAE* **2018**, *28*, e21208. [[CrossRef](#)]
17. Liu, J.; Esselle, K.P.; Hay, S.G.; Zhong, S. Effects of printed UWB antenna miniaturization on pulse fidelity and pattern stability. *IEEE Trans. Ant. Propag.* **2014**, *62*, 3903–3910. [[CrossRef](#)]
18. Haq, M.A.; Koziel, S. Feedline alterations for optimization-based design of compact super wideband MIMO antennas in parallel configuration. *IEEE Ant. Wirel. Prop. Lett.* **2019**, *18*, 1986–1990.
19. Reddy, V.V.; Sarma, N.V.S.N. Compact circularly polarized asymmetrical fractal boundary microstrip antenna for wireless applications. *IEEE Ant. Wirel. Prop. Lett.* **2014**, *13*, 118–121. [[CrossRef](#)]
20. Haq, M.A.; Koziel, S. Ground plane alterations for design of high-isolation compact wideband MIMO antenna. *IEEE Access* **2018**, *6*, 48978–48983. [[CrossRef](#)]

21. Teni, G.; Zhang, N.; Qiu, J.; Zhang, P. Research on a novel miniaturized antipodal Vivaldi antenna with improved radiation. *IEEE Ant. Wirel. Prop. Lett.* **2013**, *12*, 417–420. [[CrossRef](#)]
22. Ren, J.; Hu, W.; Yin, Y.; Fan, R. Compact printed MIMO antenna for UWB applications. *IEEE Ant. Wirel. Prop. Lett.* **2014**, *13*, 1517–1520.
23. Qin, X.; Li, Y. Compact dual-polarized cross-slot antenna with colocated feeding. *IEEE Trans. Ant. Propag.* **2019**, *67*, 7139–7143. [[CrossRef](#)]
24. Tu, W.H.; Hsu, W.H.; Chang, K. Compact 5.8-GHz rectenna using stepped-impedance dipole antenna. *IEEE Ant. Wirel. Prop. Lett.* **2007**, *6*, 282–284. [[CrossRef](#)]
25. Tao, J.; Feng, Q. Compact ultrawideband MIMO antenna with half-slot structure. *IEEE Ant. Wirel. Prop. Lett.* **2017**, *16*, 792–795. [[CrossRef](#)]
26. Reddy, B.R.S.; Vakula, D. Compact zigzag-shaped-slit microstrip antenna with circular defected ground structure for wireless applications. *IEEE Ant. Wirel. Prop. Lett.* **2015**, *14*, 678–681. [[CrossRef](#)]
27. Prajapati, P.R.; Murthy, G.G.K.; Patnaik, A.; Kartikeyan, M.V. Design and testing of a compact circularly polarised microstrip antenna with fractal defected ground structure for L-band applications. *IET Microw. Ant. Prop.* **2015**, *9*, 1179–1185. [[CrossRef](#)]
28. Park, J.P.; Han, S.M.; Itoh, T. A rectenna design with harmonic-rejecting circular-sector antenna. *IEEE Ant. Wirel. Prop. Lett.* **2004**, *3*, 52–54. [[CrossRef](#)]
29. Dahlan, A.; Kamarudin, M.R. Shorted microstrip patch antenna with parasitic element. *J. Electr. Waves. Appl.* **2010**, *24*, 327–339. [[CrossRef](#)]
30. Kasgari, M.A.; Rahim, S.K.A.; Khalily, M. Two segments compact dielectric resonator antenna for UWB application. *IEEE Ant. Wirel. Prop. Lett.* **2012**, *1*, 1533–1536.
31. Haq, M.A.; Koziel, S.; Cheng, Q.S. Miniaturization of wideband antennas by means of feed line topology alterations. *IET Microw. Ant. Prop.* **2018**, *12*, 2128–2134. [[CrossRef](#)]
32. Haq, M.A.; Koziel, S. Quantitative assessment of wideband antenna geometry modifications for size-reduction-oriented design. *AEU Int. J. Electr. Comm.* **2018**, *90*, 45–52. [[CrossRef](#)]
33. Kim, S.; Nam, S. Compact ultrawideband antenna on folded ground plane. *IEEE Trans. Ant. Propag.* **2020**, *68*, 7179–7183. [[CrossRef](#)]
34. Cui, Y.; Luo, P.; Gong, Q.; Li, R. A compact tri-band horizontally polarized omnidirectional antenna for UAV applications. *IEEE Ant. Wirel. Prop. Lett.* **2019**, *18*, 601–605. [[CrossRef](#)]
35. Johansson, D.O.; Koziel, S. Feasible space boundary search for improved optimization-based miniaturization of antenna structures. *IET Microw. Ant. Prop.* **2018**, *12*, 1273–1278. [[CrossRef](#)]
36. Johansson, D.O.; Koziel, S.; Bekasiewicz, A. EM-driven constrained miniaturization of antennas using adaptive in-band reflection acceptance threshold. *Int. J. Numer. Model.* **2019**, *32*, e2513. [[CrossRef](#)]
37. Koziel, S. Objective relaxation algorithm for reliable simulation-driven size reduction of antenna structure. *IEEE Ant. Wirel. Prop. Lett.* **2017**, *16*, 1949–1952. [[CrossRef](#)]
38. Tomasson, J.A.; Koziel, S.; Pietrenko-Dabrowska, A. Quasi-global optimization of antenna structures using principal components and affine subspace-spanned surrogates. *IEEE Access* **2020**, *8*, 50078–50084. [[CrossRef](#)]
39. Kolda, T.G.; Lewis, R.M.; Torczon, V. Optimization by direct search: New perspectives on some classical and modern methods. *SIAM Rev.* **2003**, *45*, 385–482. [[CrossRef](#)]
40. Lalbakhsh, A.; Afzal, M.U.; Esselle, K.P. Multiobjective particle swarm optimization to design a time-delay equalizer metasurface for an electromagnetic band-gap resonator antenna. *IEEE Ant. Wirel. Prop. Lett.* **2017**, *16*, 915. [[CrossRef](#)]
41. Zhao, W.J.; Liu, E.X.; Wang, B.; Gao, S.P.; Png, C.E. Differential evolutionary optimization of an equivalent dipole model for electromagnetic emission analysis. *IEEE Trans. Electromagn. Comp.* **2018**, *60*, 1635–1639. [[CrossRef](#)]
42. Rajagopalan, H.; Kovitz, J.M.; Rahmat-Samii, Y. MEMS reconfigurable optimized E-shaped patch antenna design for cognitive radio. *IEEE Trans. Ant. Propag.* **2014**, *62*, 1056–1064. [[CrossRef](#)]
43. Tziris, E.N.; Lazaridis, P.I.; Zaharis, Z.D.; Cosmas, J.P.; Mistry, K.K.; Glover, I.A. Optimized planar elliptical dipole antenna for UWB EMC applications. *IEEE Trans. Electr. Comp.* **2019**, *61*, 1377–1384. [[CrossRef](#)]
44. Singh, U.; Rattan, M. Design of thinned concentric circular antenna arrays using firefly algorithm. *IET Microw. Ant. Prop.* **2014**, *8*, 894–900. [[CrossRef](#)]
45. Koziel, S.; Ogurtsov, S.; Cheng, Q.S.; Bandler, J.W. Rapid EM-based microwave design optimization exploiting shape-preserving response prediction and adjoint sensitivities. *IET Microw. Ant. Prop.* **2014**, *8*, 775–781. [[CrossRef](#)]
46. Hassan, E.; Noreland, D.; Augustine, R.; Wadbro, E.; Berggren, M. Topology optimization of planar antennas for wideband near-field coupling. *IEEE Trans. Ant. Prop.* **2015**, *63*, 4208–4213. [[CrossRef](#)]
47. Koziel, S.; Pietrenko-Dabrowska, A. Expedited optimization of antenna input characteristics with adaptive Broyden updates. *Eng. Comp.* **2019**, *37*, 851–862. [[CrossRef](#)]
48. Koziel, S.; Pietrenko-Dabrowska, A. Expedited feature-based quasi-global optimization of multi-band antennas with Jacobian variability tracking. *IEEE Access* **2020**, *8*, 83907–83915. [[CrossRef](#)]
49. Cervantes-González, J.C.; Rayas-Sánchez, J.A.; López, C.A.; Camacho-Pérez, J.R.; Brito-Brito, Z.; Chávez-Hurtado, J.L. Space mapping optimization of handset antennas considering EM effects of mobile phone components and human body. *Int. J. RF Microw. CAE* **2016**, *26*, 121–128. [[CrossRef](#)]

50. Koziel, S.; Ogurtsov, S. *Antenna Design by Simulation—Driven Optimization*; Springer: New York, NY, USA, 2014.
51. Easum, J.A.; Nagar, J.; Werner, P.L.; Werner, D.H. Efficient multi-objective antenna optimization with tolerance analysis through the use of surrogate models. *IEEE Trans. Ant. Prop.* **2018**, *66*, 6706–6715. [[CrossRef](#)]
52. Bandler, J.W.; Cheng, Q.S.; Dakroury, S.A.; Mohamed, A.S.; Bakr, M.H.; Madsen, K.; Sondergaard, J. Space mapping: The state of the art. *IEEE Trans. Microw. Theory Tech.* **2004**, *52*, 337–361. [[CrossRef](#)]
53. Zhang, C.; Feng, F.; Gongal-Reddy, V.; Zhang, Q.J.; Bandler, J.W. Cognition-driven formulation of space mapping for equal-ripple optimization of microwave filters. *IEEE Trans. Microw. Theory Techn.* **2015**, *63*, 2154–2165. [[CrossRef](#)]
54. Koziel, S.; Leifsson, L. *Simulation—Driven Design by Knowledge—Based Response Correction Techniques*; Springer: New York, NY, USA, 2016.
55. Koziel, S.; Unnsteinsson, S.D. Expedited design closure of antennas by means of trust-region-based adaptive response scaling. *IEEE Antennas Wirel. Prop. Lett.* **2018**, *17*, 1099–1103. [[CrossRef](#)]
56. Koziel, S. Fast simulation-driven antenna design using response-feature surrogates. *Int. J. RF Microw. CAE* **2015**, *25*, 394–402. [[CrossRef](#)]
57. Koziel, S.; Ogurtsov, S.; Zieniutycz, W.; Sorokosz, L. Expedited design of microstrip antenna subarrays using surrogate-based optimization. *IEEE Ant. Wirel. Prop. Lett.* **2014**, *13*, 635–638. [[CrossRef](#)]
58. Hassan, A.K.S.O.; Etman, A.S.; Soliman, E.A. Optimization of a novel nano antenna with two radiation modes using kriging surrogate models. *IEEE Photonic J.* **2018**, *10*, 4800807. [[CrossRef](#)]
59. Barmuta, P.; Ferranti, F.; Gibiino, G.P.; Lewandowski, A.; Schreurs, D.M.M.P. Compact behavioral models of nonlinear active devices using response surface methodology. *IEEE Trans. Microw. Theory Tech.* **2015**, *63*, 56–64. [[CrossRef](#)]
60. Rawat, A.; Yadav, R.N.; Shrivastava, S.C. Neural network applications in smart antenna arrays: A review. *AEU Int. J. Elec. Comm.* **2012**, *66*, 903–912. [[CrossRef](#)]
61. Petrocchi, A.; Kaintura, A.; Avolio, G.; Spina, D.; Dhaene, T.; Raffo, A.; Schreurs, D.M.P.-P. Measurement uncertainty propagation in transistor model parameters via polynomial chaos expansion. *IEEE Microw. Wirel. Comp. Lett.* **2017**, *27*, 572–574. [[CrossRef](#)]
62. Cai, J.; King, J.; Yu, C.; Liu, J.; Sun, L. Support vector regression-based behavioral modeling technique for RF power transistors. *IEEE Microw. Wirel. Comp. Lett.* **2018**, *28*, 428–430. [[CrossRef](#)]
63. De Villiers, D.I.L.; Couckuyt, I.; Dhaene, T. Multi-objective optimization of reflector antennas using kriging and probability of improvement. In Proceedings of the 2017 IEEE International Symposium on Antennas and Propagation & USNC/URSI National Radio Science Meeting, San Diego, CA, USA, 9–14 July 2017.
64. Tak, J.; Kantemur, A.; Sharma, Y.; Xin, H. A 3-D-printed W-band slotted waveguide array antenna optimized using machine learning. *IEEE Ant. Wirel. Prop. Lett.* **2018**, *17*, 2008–2012. [[CrossRef](#)]
65. Koziel, S.; Pietrenko-Dabrowska, A. *Performance—Driven Surrogate Modeling of High—Frequency Structures*; Springer: New York, NY, USA, 2020.
66. Koziel, S.; Mosler, F.; Reitzinger, S.; Thoma, P. Robust microwave design optimization using adjoint sensitivity and trust regions. *Int. J. RF Microw. CAE* **2012**, *22*, 10–19. [[CrossRef](#)]
67. Koziel, S.; Pietrenko-Dabrowska, A. Reduced-cost electromagnetic-driven optimization of antenna structures by means of trust-region gradient-search with sparse Jacobian updates. *IET Microw. Ant. Prop.* **2019**, *13*, 1646–1652. [[CrossRef](#)]
68. Koziel, S.; Unnsteinsson, S.D.; Bekasiewicz, A. Low-fidelity model considerations for simulation-based optimization of miniaturized wideband antennas. *IET Microw. Ant. Prop.* **2018**, *12*, 1613–1619. [[CrossRef](#)]
69. Koziel, S.; Ogurtsov, S. Model management for cost-efficient surrogate-based optimization of antennas using variable-fidelity electromagnetic simulations. *IET Microw. Ant. Prop.* **2012**, *6*, 1643–1650. [[CrossRef](#)]
70. Ullah, U.; Koziel, S.; Mabrouk, I.B. Rapid re-design and bandwidth/size trade-offs for compact wideband circular polarization antennas using inverse surrogates and fast EM-based parameter tuning. *IEEE Trans. Ant. Prop.* **2019**, *68*, 81–89. [[CrossRef](#)]
71. Conn, A.R.; Gould, N.I.M.; Toint, P.L. *Trust Region Methods*; MPS-SIAM Series on Optimization: Philadelphia, PA, USA, 2000.
72. Su, Y.; Li, J.; Fan, Z.; Chen, R. Shaping optimization of double reflector antenna based on manifold mapping. In Proceedings of the 2017 International Applied Computational Electromagnetics Society Symposium (ACES 2017), Suzhou, China, 1–2 August 2017.
73. Liu, B.; Koziel, S.; Ali, N. SADEA-II: A generalized method for efficient global optimization of antenna design. *J. Comp. Design Eng.* **2017**, *4*, 86–97. [[CrossRef](#)]
74. Koziel, S.; Bekasiewicz, A.; Couckuyt, I.; Dhaene, T. Efficient multi-objective simulation-driven antenna design using co-kriging. *IEEE Trans. Antennas Prop.* **2014**, *62*, 5900–5905. [[CrossRef](#)]
75. Jacobs, J.P.; Koziel, S. Two-stage framework for efficient Gaussian process modeling of antenna input characteristics. *IEEE Trans. Antennas Prop.* **2014**, *62*, 706–713. [[CrossRef](#)]
76. Alsath, M.G.N.; Kanagasabai, M. Compact UWB monopole antenna for automotive communications. *IEEE Trans. Ant. Prop.* **2015**, *63*, 4204–4208. [[CrossRef](#)]
77. Koziel, S.; Bekasiewicz, A. Low-cost multi-objective optimization of antennas using Pareto front exploration and response features. In Proceedings of the 2016 IEEE International Symposium on Antennas and Propagation (APSURSI 2016), Fajardo, Puerto Rico, 26 June–1 July 2016.
78. Haq, M.A.; Koziel, S. Simulation-based optimization for rigorous assessment of ground plane modifications in compact UWB antenna design. *Int. J. RF Microw. CAE* **2018**, *28*, e21204. [[CrossRef](#)]